Relative mobility of screw versus edge dislocations controls the ductile-to-brittle transition in metals

Yan Lu[a], Yu-Heng Zhang[a], En Ma[b], and Wei-Zhong Han[a,1]

[a]Center for Advancing Materials Performance from the Nanoscale, State Key Laboratory for Mechanical Behavior of Materials, Xi'an Jiaotong University, Xi'an 710049, People's Republic of China; and [b]Center for Alloy Innovation and Design, State Key Laboratory for Mechanical Behavior of Materials, Xi'an Jiaotong University, Xi'an 710049, People's Republic of China

Edited by Alexis T. Bell, University of California, Berkeley, CA, and approved August 9, 2021 (received for review June 8, 2021)

Body-centered cubic metals including steels and refractory metals suffer from an abrupt ductile-to-brittle transition (DBT) at a critical temperature, hampering their performance and applications. Temperature-dependent dislocation mobility and dislocation nucleation have been proposed as the potential factors responsible for the DBT. However, the origin of this sudden switch from toughness to brittleness still remains a mystery. Here, we discover that the ratio of screw dislocation velocity to edge dislocation velocity is a controlling factor responsible for the DBT. A physical model was conceived to correlate the efficiency of Frank–Read dislocation source with the relative mobility of screw versus edge dislocations. A sufficiently high relative mobility is a prerequisite for the coordinated movement of screw and edge segments to sustain dislocation multiplication. Nanoindentation experiments found that DBT in chromium requires a critical mobility ratio of 0.7, above which the dislocation sources transition from disposable to regeneratable ones. The proposed model is also supported by the experimental results of iron, tungsten, and aluminum.

brittle | ductile | dislocation | mobility

The ductile-to-brittle transition (DBT) is a ubiquitous feature in body-centered cubic (BCC) metals (1). Below a critical temperature, termed the ductile-to-brittle transition temperature (DBTT), the plasticity of BCC metals displays an abrupt transition from ductile deformation to cleavage brittle fracture (1–9), limiting the temperature window for the utilization of these metals (1–9). Therefore, a thorough understanding of the mechanism controlling the DBT in BCC metals is essential for their broader applications.

The brittleness/toughness of a material (i.e., its resistance to crack propagation) (10), depends on the dislocation activities near the crack tip (11). Crack tip plasticity, which slows down or arrests the advancing crack, consists of two distinct processes: nucleation of dislocations at or near the crack tip and their gliding away from the crack (10–16). As such, the DBT properties of BCC metals can be traced back to the nucleation and gliding of a/2⟨111⟩ screw dislocations. In BCC metals, these screw dislocations have a dissociated, three-dimensional core structure and a threefold symmetry under ambient conditions (17, 18). For dislocation nucleation, dislocation sources may have a hard time operating at low temperatures (19). For dislocation glide, an intrinsic resistance, the Peierls stress, has to be overcome (20, 21). Therefore, there is a debate as to whether screw dislocation nucleation or glide controls the DBT (11–14). The DBTT strongly depends on the loading rates, microstructures, and impurities (22–24). The temperature-dependence of the fracture toughness and the strain rate dependence of a DBT reveals that the activation energy for the DBT is close to that for double-kink formation on the screw dislocation (16, 25); this is a hint that DBT is controlled by screw dislocation mobility. However, there is no compelling explanation as to why the smooth/gradual temperature-dependent kink-pair formation always gives rise to an abrupt DBT. A convincing and quantitative link between dislocation properties and the DBT still remains elusive (26–29).

In this report, we have used high-temperature nanoindentation to gauge DBT in chromium (Cr) and quantify the relative mobility of screw versus edge dislocation. We then propose a physical model to correlate the efficiency of dislocation source to the relative mobility of screw versus edge dislocations. Our results indicate that a sudden change in dislocation multiplication efficiency can well explain the abrupt transition characteristics of DBT.

Results

High-purity polycrystalline Cr was used as model material. The microstructures of Cr are shown in *SI Appendix*, Fig. S1. The initial defect density is very low. Nanoindentation was performed on selected Cr grains in the temperature range of 20 °C to 190 °C (*SI Appendix*, Fig. S2). Fig. 1*A* shows the temperature-dependent load–depth curves of a [124] grain. Upon loading, the indentation depth increases linearly with increasing load (30). The elastic part of the load–depth follows the Hertzian relation (31). At a critical load of 700 ± 150 N, a sudden displacement burst occurs, known as the "pop-in" (32), which indicates the transition from elasticity to plasticity (30). With further-increased pressure, the load–depth curve fluctuates for tests above 70 °C but is still smooth for tests below 70 °C, as shown in Fig. 1*B*. During load holding, the indentation depth also increases with time and shows two distinct regions: a fast stage before 0.5 s and a stable creep afterward, as plotted in Fig. 1*C*.

The maximum shear stress, τ_{max}, at which dislocations nucleate underneath the indenter, are plotted in Fig. 1*D* as a function of temperature. Overall, the maximum shear stress decreases with increasing temperature, but there is no critical turning point.

Significance

This work uncovers the mystery of ductile-to-brittle transition (DBT) in body-centered cubic (BCC) metals. Temperature-dependent dislocation mobility and dislocation nucleation have been proposed as the potential factors responsible for the DBT. However, there is no compelling explanation as to why the smooth/gradual temperature-dependent kink-pair formation always gives rise to an abrupt DBT. We discover that the ratio of screw dislocation velocity to edge dislocation velocity is a controlling factor responsible for the DBT. A sufficiently high relative mobility is a prerequisite for the coordinated movement of screw and edge segments to sustain dislocation multiplication. The study offers fundamental insights into the deformation mechanism of BCC metals.

Author contributions: W.-Z.H. designed research; Y.L. performed research; Y.L., Y.-H.Z., E.M., and W.-Z.H. analyzed data; and Y.L., E.M., and W.-Z.H. wrote the paper.

The authors declare no competing interest.

This article is a PNAS Direct Submission.

[1]To whom correspondence may be addressed. Email: wzhanxjtu@mail.xjtu.edu.cn.

This article contains supporting information online at https://www.pnas.org/lookup/suppl/doi:10.1073/pnas.2110596118/-/DCSupplemental.

Published September 7, 2021.

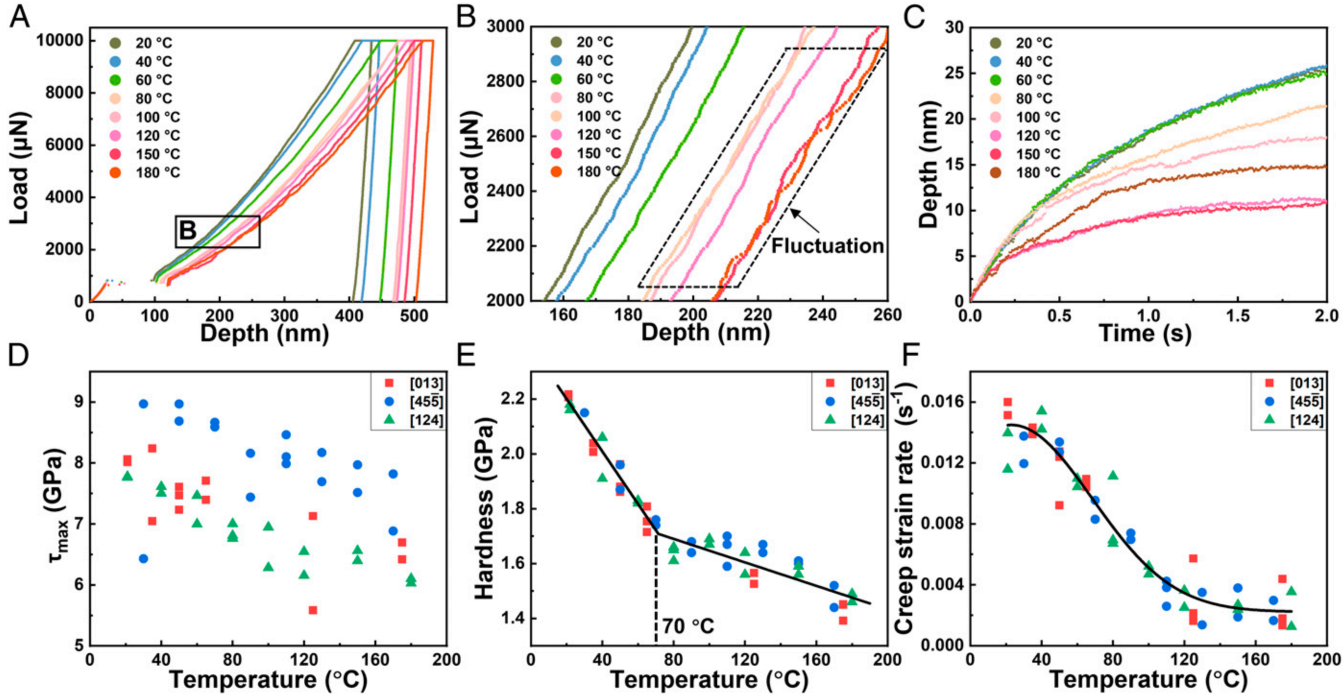

Fig. 1. Nanoindentation behavior of Cr. (*A*) Loading curves of Cr grain with [124] orientation. (*B*) Enlarged image of the area marked in *A*. (*C*) Depth versus time curves during the load holding stage. (*D*) Pop-in shear stress as a function of temperature. (*E*) Variation in hardness with testing temperature. (*F*) Temperature-dependent creep strain rate.

Hardness can be determined according to $H = \frac{Pmax}{Ac}$ (33), where H is hardness, $P_{\max}$ is the maximum applied load, and A_c is the contact area at maximum load. Fig. 1*E* plots the hardness versus temperature for tests in grains with orientations of [013], [45$\bar{5}$], and [124], respectively. The hardness shows two stages: it decreases with increasing temperature below 70 °C and then switches into a stage with a weak temperature dependence. An obvious turn in hardness is evident at 70 °C. This transition temperature in nanoindentation is very close to the DBTT of Cr determined under Charpy test (34). The sharp turn reveals the existence of a switch in deformation mechanism near DBTT, which could then possibly be responsible for the DBT.

The creep strain rate ($\dot{\varepsilon}_{\mathrm{H}}$) can be obtained by $\dot{\varepsilon}_H = \frac{1}{h}\frac{dh}{dt}$ (35, 36), where h and t are the instantaneous indentation depth and time, respectively. Fig. 1*F* shows the stable creep strain rate (after load holding for 1.5 s) as a function of temperature. In between the top and bottom plateaus, the creep strain rate goes through a transition region, with a midway point again at ~70 °C. The distinctly different behaviors below and above ~70 °C in the load–depth curves, hardness, and creep rate of Cr all reflect a major switch in the underlying dislocation behaviors.

To explore the mechanism of DBT, we studied the dislocation structures produced underneath the indentations just after the pop-in in [45$\bar{5}$] orientated grains below (30 °C), at (70 °C), and above (170 °C) the critical temperature for DBT (Fig. 2). Fig. 2 *A* and *D* show dislocation structures underneath the indent at 30 °C. The pop-in curve is displayed in Fig. 2*E*. The Burgers vectors of dislocations are highlighted in different colors in Fig. 2*A*. There are two kinds of dislocations with different Burgers vectors: ±1/2[11$\bar{1}$] in red and ±1/2[1$\bar{1}$1] in blue. Both screw dislocations and edge dislocations are observed, as marked in Fig. 2*A*. To mediate the pop-in strain, three slip systems were activated, two of which were along the same [11$\bar{1}$] direction and the other along the [1$\bar{1}$1] direction. The nucleated dislocations have a mixed character. Upon slipping forward, the fraction of edge dislocations increases, while that of the screw segments decreases, as manifested by the short, straight dislocations in Fig. 2*A*. In the region far from the indentation, only pure-edge dislocations remain.

Fig. 2 *B* and *F* show the dislocation structures formed after pop-in loading (Fig. 2*G*) at 70 °C. Similarly, three traces of dislocations were observed in Fig. 2*B*. Most emitted dislocations are straight edge dislocations. In another test at 70 °C, the fraction of mixed and screw dislocations was higher than that in Fig. 2*B*, as shown in *SI Appendix*, Fig. S5. These observations indicate that the dislocations should have experienced a transition in mobility at 70 °C.

Fig. 2 *C* and *H* show the dislocation structures produced after pop-in loading (Fig. 2*I*) at 170 °C. Both the dislocations near the indentation and far away from it are curved and entangled, indicating that most dislocations now have a mixed character. Only a few pure-edge dislocations can be identified in Fig. 2*C*. Dislocations with distinct Burgers vectors are connected to each other (Fig. 2*H*), indicating dislocation reactions. Details for determining the Burgers vectors of the dislocations are displayed in *SI Appendix*, Figs. S3–S7. The characteristics of dislocations has a clear temperature-dependence. Easy glide edge dislocations prevail below the DBTT, while mixed dislocations dominate plasticity above it.

Fig. 3*A* shows another example of dislocation structures underneath an indent at 70 °C. By chance, there is a small-angle grain boundary (SAGB) ~4 μm away from the indentation. In this case, the nucleation and emission of dislocations (Fig. 3*B*) are similar to Fig. 2, while the gliding of dislocations is obstructed by the SAGB. As shown in Fig. 3*A*, three traces of dislocations are triggered. The two downward traces of dislocations met at the GB and then partially transmitted through it. A pile-up of dislocations is formed in front of the SAGB, increasing the back stress for subsequent dislocations. A large fraction of edge dislocations can still be identified in Fig. 3*A*. The fraction of mixed and screw components is increased compared to Fig. 2*B*.

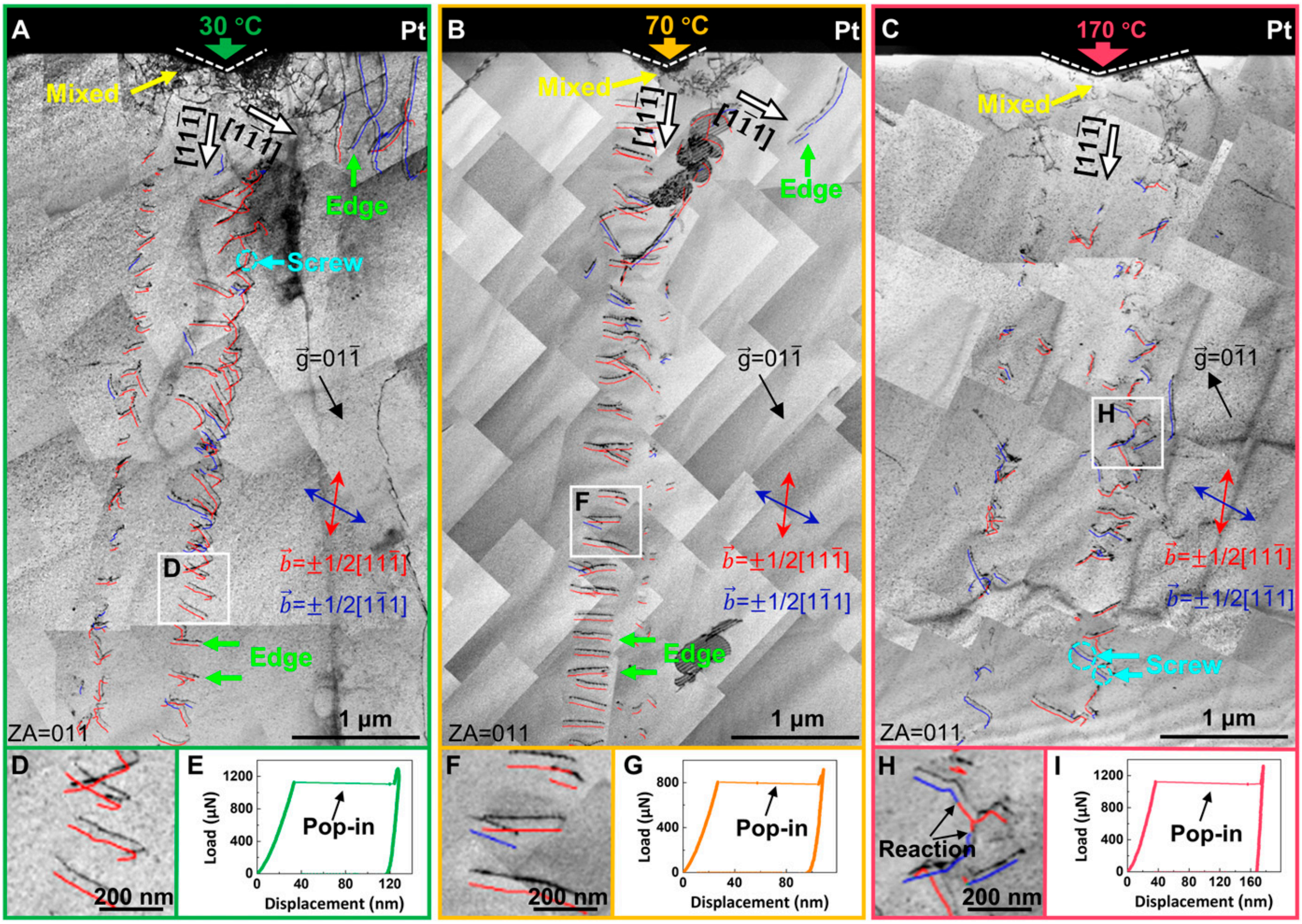

Fig. 2. Dislocation structures underneath indentation in $[45\bar{5}]$ grain. Dislocation structures after indentation at (*A*) 30 °C, (*B*) 70 °C, and (*C*) 170 °C. (Scale bars, 1 μm.) *D*, *F*, and *H* highlight dislocation structures in white squares. (Scale bars, 200 nm.) *E*, *G*, and *I* are pop-in curves.

Discussion

In this work, the transition temperature (70 °C) observed in nanoindentation tests (datasets of nanoindentation hardness, load–depth curves, and the creep rate) is in the neighborhood of the experimental DBTT of Cr, measured using Charpy test in the literature (34): for example, fine-grained Cr has a DBTT at 90 °C, whereas coarse-grained Cr shows a DBTT of 30 °C. Therefore, the transition observed in our tests is very likely to be responsible for the change in dislocation mechanism underlying the DBT. This proposition is supported by the observation that the features of the dislocations under the indent are indeed different below and above 70 °C, an indication that around this temperature, the dislocation mechanism is indeed different, which is expected to be an origin of the DBT observed under fracture load/mode. To gain physical insight, as shown above, we have monitored quantitatively the velocity of edge versus screw dislocations at different temperatures, which reveals a specific mechanism underlying the DBT.

During the pop-in loadings in Figs. 2 and 3, dislocations nucleate and emit underneath the indenter within 0.01 s. We estimate the average dislocation velocity (ν) using the Orowan equation (37):

$$\nu = \frac{\dot{\varepsilon}}{\rho b}, \qquad [1]$$

where b is the magnitude of the Burgers vector, ρ is the dislocation density, and $\dot{\varepsilon}$ can be obtained via $\dot{\varepsilon}_H = \frac{1}{h}\frac{dh}{dt}$ (35, 36). Fig. 3*B* shows the dislocation velocity as a function of temperature. The average dislocation velocity increases rapidly from 30 °C to 70 °C and then slowly increases at temperatures above DBTT. As a comparison, for the test with a SAGB at 70 °C, the average velocity of dislocations (0.012 m/s) is half of the dislocation velocity (0.027m/s) without the influence of SAGB at the same temperature. Hence a high fraction of GBs enhances the DBTT (28).

The change in the dislocation mobility is also reflected by the evolving relative fraction of edge and screw dislocations, as shown in Fig. 3*C*. A mixed dislocation can be divided into an edge segment and a screw segment according to the angle between the Burgers vector and dislocation line. Below the DBTT, since the velocity of screw dislocation is much smaller than that of edge dislocation, the remaining screw part in the dislocation decreases, and eventually, only pure-edge dislocations survive (Fig. 2). For tests above the DBTT, the mobility of screw segments is comparable with that of the edge dislocations; hence, the screw segments can slip forward as far as the edge dislocations (Fig. 2*C* and *SI Appendix*, Fig. S5). As a result, the dislocation structures include ∼50% edge segments and 50% screw segments.

For Cr, its critical temperature T_c is 170 °C, at which screw and edge dislocations have equal mobility (38), such as $\nu_s = \nu_e =$ 0.0316 m/s according to Fig. 3*B*. Based on the fraction of screw and edge segments, we can also estimate their mobility at lower testing temperatures, as plotted in Fig. 3*B*. The edge dislocation velocity remains constant, while the screw dislocation mobility

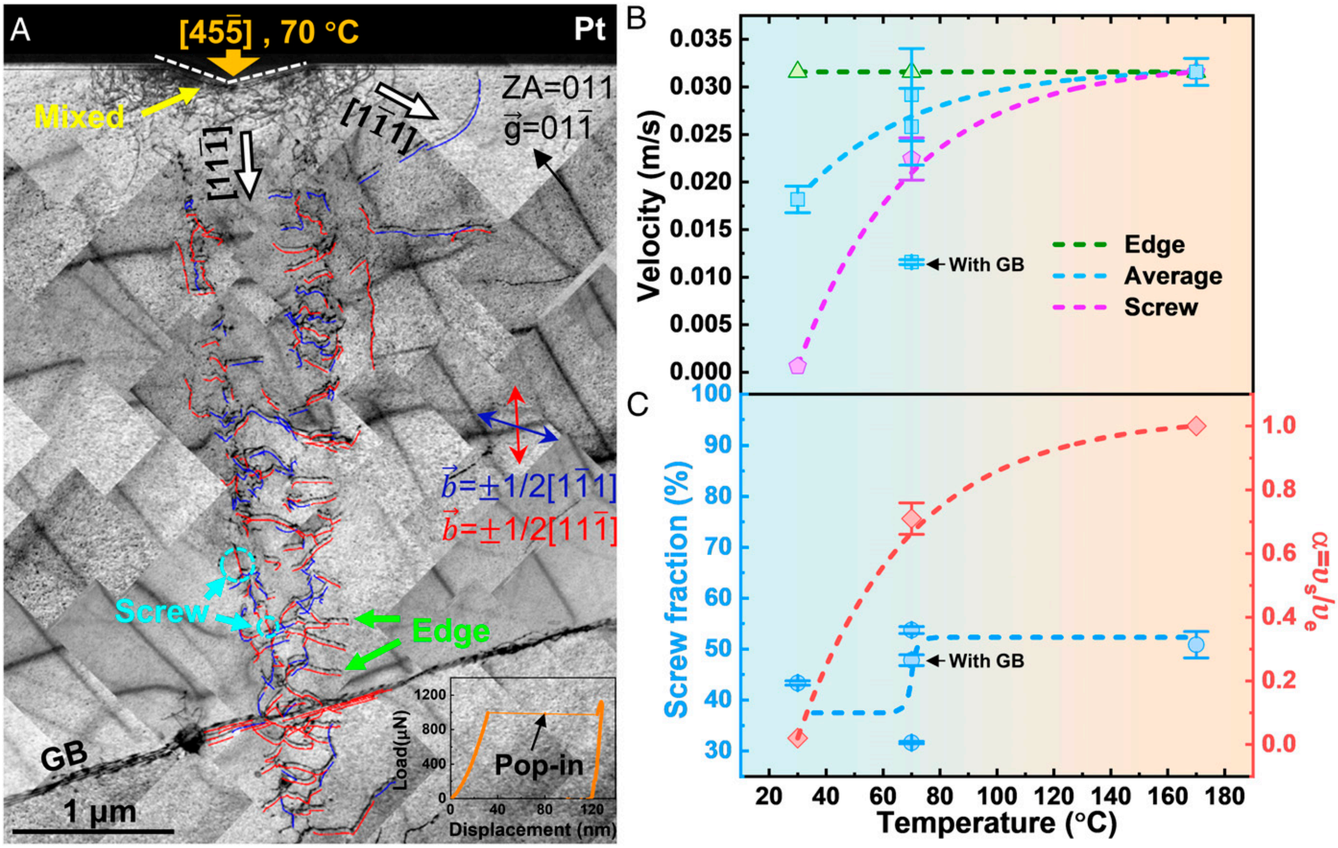

Fig. 3. Characteristics and mobility of dislocations. (*A*) Dislocation structures after pop-in load at 70 °C in a [45$\bar{5}$] grain with a SAGB. (Scale bar, 1 μm.) Temperature-dependent dislocation velocity (*B*) and screw segment fraction and α (*C*).

increases with increasing temperature. At 30 °C, the mobility of edge dislocations is at least one order of magnitude higher than that for screw dislocations. Notably, the relative dislocation mobility ($\alpha = v_s/v_e$) is also a strong function of the testing temperature, and at a critical value, $\alpha = 0.7$, Cr shows the DBT, as shown in Fig. 3*C*. Note that the mobility ratio of screw to edge dislocations correlates with the dislocation configuration in Fig. 2 and the screw component fraction in Fig. 3*C*.

Below DBTT, screw dislocations have much lower mobility than edge dislocations, which appears to be the origin of brittleness. At DBTT, the dislocation mobility swings between brittle and ductile behavior; thus, two distinct characteristics of dislocations are observed at 70 °C in two separate tests (Fig. 2*B* and *SI Appendix*, Fig. S5), but the average dislocation velocity for both cases increases. Above DBTT, the glide speed of the screw dislocations becomes comparable with that of the edge dislocations (38); thus, the plasticity can be well coordinated.

The screw dislocation velocity also influences the cross-slip rate. Below 70 °C, the dislocation structures are relatively simple (Fig. 2*A*), resulting from prismatic punching of dislocation loops (39–41). However, the dislocation structure above 70 °C (Fig. 2*C*) is more complex and involves dislocation reactions, indicating the occurrence of cross-slip. The temperature effect on cross-slip efficacy is also a factor influencing the temperature-dependence of hardness observed in nanoindentation.

We next propose a model, as shown in Fig. 4*A*, to explain the relationships among relative dislocation mobility, Frank–Read source, and the abrupt DBT. Specifically, the sharp DBT is controlled by the availability of effective dislocation sources (11–13, 42), which was affected by the relative dislocation mobility. The velocity ratio $\alpha = v_s/v_e$ determines the efficiency of dislocation sources, holding the key to produce a sufficiently large number of dislocations to carry the plasticity.

To see this, we begin with the bowing-out of an edge dislocation shown in Fig. 4*A* below DBTT, where $v_e \gg v_s$. In this case, the bowing part of the dislocation can be a dislocation source (mainly edge part glide); however, this is a disposable source with very low efficiency. Fig. 4 *B*–*D* show different scenarios to illustrate how $\alpha = v_s/v_e$ affects the efficiency of Frank–Read source. Again, as seen in Fig. 4*B*, an edge dislocation bowing out into a half loop with only edge dislocation glide would make a highly efficient Frank–Read source if $v_e = v_s$. However, $v_e > v_s$ for most metals because of their distinct core structures (17). In an extreme case of $v_s = 0$, for the ensuing further bow-out as shown in Fig. 4*C*, the half loop expands forward with distance of x, forming a half ellipse, but there is no glide of a screw dislocation segment. The absence of side glide suppresses the repeated operation of the Frank–Read source (19, 43). In general, the pink region is the area (A_{edge}) swept by the edge dislocation in this process. With some v_s, the bowing-out of half loop would form a green half ellipse in Fig. 4*D*, with both a forward glide distance of x and a side glide distance of y. The marked green area is the region (A_{screw}) swept by the screw dislocation. Only when the area swept by the screw dislocation is larger than the area swept by the edge dislocation can the bowing part immediately evolve into a Frank–Read source.

This efficient operation of the Frank–Read source requires $0 < x < r$, where r is the dislocation source radius. Otherwise, for $x > r$, the dislocation source is a low-efficiency disposable one. Since

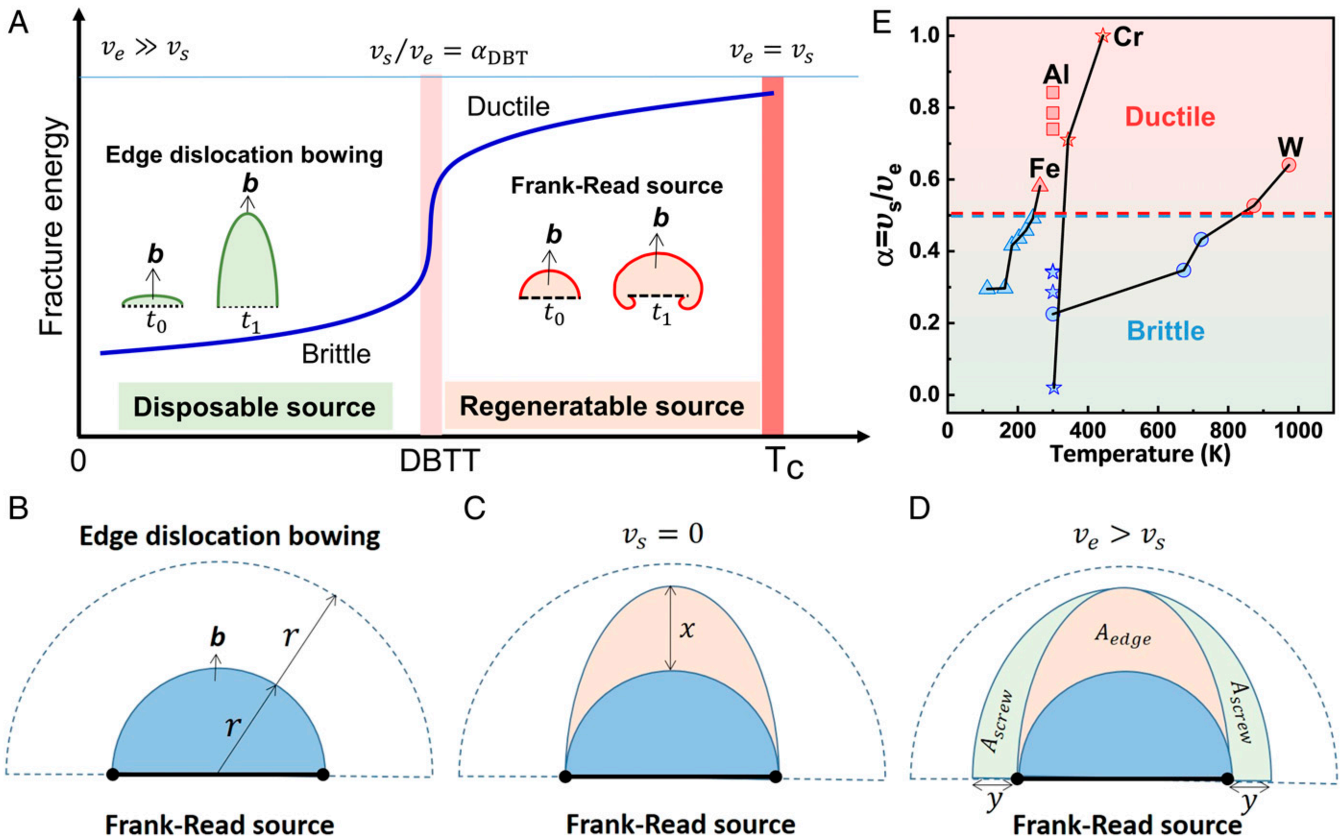

Fig. 4. Dislocation relative mobility and efficiency of Frank–Read source. (*A*) Dislocation relative mobility determines the efficiency of dislocation source. (*B*) Bowing out an edge dislocation to form a half loop. (*C*) Bowing out the half loop if $v_s = 0$. (*D*) Bowing out the half loop with side glide ($v_s > 0$). (*E*) Variation of α with temperature for Cr, Al, W, and Fe according to in *SI Appendix*, Figs. S3 and S8.

$$\alpha = \frac{v_s}{v_e} = \frac{y}{x} = \frac{r}{r + x}, \qquad [2]$$

this $x < r$ criterion translates to $\alpha_{DBT} \geq 0.5$ as the critical requirement for an effective Frank–Read source to operate. In current experiments, we find that the required relative mobility of dislocations is around 0.7 for dislocation free Cr. This value falls in the predicted range of $\alpha_{DBT} > 0.5$. In other words, ample plasticity requires at least $\alpha > 0.5$. We compare the α model with data of Cr, Al, Fe, and W collected from Fig. 3*C* and *SI Appendix*, Fig. S8, as plotted in Fig. 4*E*. All these metals are brittle when $\alpha < 0.5$, but they transition into a ductile regime at a $\alpha_{DBT} > 0.5$. Above DBTT, α increases toward 1, guaranteeing the ductile behavior.

For BCC metals, the faster the glide speed of screw dislocations, the higher the efficiency of Frank–Read source and cross-slip and hence the better the ability to coordinate plasticity. Below the DBTT, the screw dislocation mobility increases with increasing temperature, making the hardness strongly temperature-dependent (refer to Fig. 1*E* below 70 °C). However, in this regime, the relative mobility of dislocation is always low; thus, the samples show brittleness. Once above the DBTT, screw dislocations glide much more easily, and numerous high-efficiency Frank–Read sources and easy cross-slips boost ductile deformation, hence the hardness displays a weak temperature-dependence. Similarly, the change in dislocation relative mobility can also explain the transition from smooth to fluctuating load-displacement curves in Fig. 1*B*. Above the DBTT, the mobility of screw and edge dislocations are comparable, high-efficiency Frank–Read sources, and easy cross-slips produce a high density of dislocations; therefore, the plastic deformation can be well coordinated. Local dislocation avalanche events occur, which induce serrations in the loading curves. Below the DBTT, existing Frank–Read sources are of low efficiency; thus, dislocations are insufficient to carry plasticity when the load reaches the maximum. The dislocations slowly slip forward during load holding, which is the origin of the sustained creep strain rate for tests below the DBTT in Fig. 1*F*. A sudden change in dislocation multiplication mechanism can well explain the abrupt transition characteristics of DBT

In summary, nanoindentation hardness as a function of test temperature can be used to gauge the DBT and DBTT in metals. Adequate plasticity to avoid brittleness requires profuse dislocation generation/activities. The latter then demands effective Frank–Read sources and easy cross-slip, which in turn relies on a sufficiently high screw-to-edge velocity ratio to operate efficiently.

Materials and Methods

Materials. A bulk polycrystalline piece of Cr (purity > 99.99%) was prepared via 1,250 °C annealing for 12 h inside an argon atmosphere. Polycrystalline Cr sample with an average grain size of 200 μm was first mechanically ground and polished with silicon carbide paper and diamond suspensions. To reduce the initial dislocation density and minimize tiny surface damage resulting from mechanical polishing, the samples were further electrolytically etched with a mixture of 10 wt% sodium hydroxide and 90 wt% water at 15 V for 2 min and then electrolytically polished with a mixture of 10 vol% perchloric acid and 90 vol% alcohol at 50 V for 5 min at approximately −40 °C. The orientation of the grains was determined using electron backscattered diffraction (EBSD) method.

High-Temperatrue Nanoindentation. Nanoindentation was performed using a Hysitron TI950 Triboindenter with a Berkovich indenter. Two types of nanoindentation tests were conducted to study the effect of temperature on the plastic deformation behavior of Cr. First, load-controlled indentation tests at a constant loading rate of 2 mN/s with a 2-s holding segment at a peak of 10 mN were conducted at various temperatures in a single grain. The orientation of the grains was determined using EBSD. The indent morphology was characterized using scanning electron microscope (SEM) (*SI Appendix*, Fig. S1). Second, the indentation test was performed with a constant loading rate of 150 μN/s at 30 °C, 70 °C, and 170 °C. When a pop-in event appears, the loading is stopped immediately. In this case, the dislocation structures formed during pop-in loading would remain. All tests were conducted from high temperature to low temperature. Before indentation, the sample was heated to the target temperature and held for at least 30 mins, then the indenter was shifted to touch the sample surface and equilibrated for another 30 min.

Microstructure Characterization. The microstructures after indentation were characterized using a Hitachi SU6600 SEM, while typical deformation microstructures beneath the indentation were examined by cutting thin foils using a focused ion beam. To minimize Ga+ damage, flashing electrolytic polishing of the lift-out sample was performed in a solution of 10 vol% perchloric acid at a voltage of 40 V and at −40 °C for 70 ms. The characteristics of dislocations were investigated using a JEOL 2100F transmission electron microscope (200 kV) under different two-beam conditions. The average dislocation density is obtained by counting the local dislocation density in three regions, each with dimensions of 1.5 μm × 1.5 μm, at different distances from the indentation.

Data Availability. All study data are included in the article and/or *SI Appendix*.

ACKNOWLEDGMENTS. Y.L. appreciates the assistance of K. Wu, P. C. Zhang, and D. L. Zhang in this study. E.M. acknowledges Xi'an Jiaotong University for supporting his work at Center for Alloy Innovation and Design. This research was supported by the National Natural Science Foundation of China (Grants 51971170 and 51922082), the 111 Project of China (Grant BP2018008), and the Innovation Project of Shaanxi Province (Grant 2017KTPT-12).

1. J. W. Christian, Some surprising features of the plastic deformation of body-centered cubic metals and alloys. *Metall. Trans., A, Phys. Metall. Mater. Sci.* **14**, 1237–1256 (1983).
2. S. G. Roberts, A. S. Booth, P. B. Hirsch, Dislocation activity and brittle-ductile transitions in single crystals. *Mater. Sci. Eng. A* **176**, 91–98 (1994).
3. P. Gumbsch, J. Riedle, A. Hartmaier, H. F. Fischmeister, Controlling factors for the brittle-to-ductile transition in tungsten single crystals. *Science* **282**, 1293–1295 (1998).
4. J. Marian, W. Cai, V. V. Bulatov, Dynamic transitions from smooth to rough to twinning in dislocation motion. *Nat. Mater.* **3**, 158–163 (2004).
5. M. Tanaka, E. Tarleton, S. G. Roberts, The brittle-ductile transition in single-crystal iron. *Acta Mater.* **56**, 5123–5129 (2008).
6. A. A. N. Németh, J. Reiser, D. E. J. Armstrong, M. Rieth, The nature of the brittle-to-ductile transition of ultra fine grained tungsten (W) foil. *Int. J. Refract. Met. Hard Mater.* **50**, 9–15 (2015).
7. A. Giannattasio, Z. Yao, E. Tarleton, S. G. Roberts, Brittle-ductile transitions in polycrystalline tungsten. *Philos. Mag.* **90**, 3947–3959 (2010).
8. J. Ast *et al*., The brittle-ductile transition of tungsten single crystals at the micro-scale. *Mater. Des.* **152**, 168–180 (2018).
9. J. Kappacher, A. Leitner, D. Kiener, H. Clemens, V. Maier-Kiener, Thermally activated deformation mechanisms and solid solution softening in W-Re alloys investigated via high temperature nanoindentation. *Mater. Des.* **189**, 108499 (2020).
10. L. Huang *et al*., In situ scanning transmission electron microscopy observations of fracture at the atomic scale. *Phys. Rev. Lett.* **125**, 246102 (2020).
11. J. R. Rice, R. Thomson, Ductile versus brittle behaviour of crystals. *Philos. Mag.* **29**, 73–97 (1974).
12. J. Samuels, S. G. Roberts, The brittle–ductile transition in silicon. I. Experiments. *Proc. R. Soc. Lond. A Math. Phys. Sci.* **421**, 1–23 (1989).
13. M. Khantha, D. P. Pope, V. Vitek, Dislocation screening and the brittle-to-ductile transition: A Kosterlitz-Thouless type instability. *Phys. Rev. Lett.* **73**, 684–687 (1994).
14. A. Hartmaier, P. Gumbsch, Thermal activation of crack-tip plasticity: The brittle or ductile response of a stationary crack loaded to failure. *Phys. Rev. B Condens. Matter Mater. Phys.* **71**, 024108 (2005).
15. M. Tanaka, A. J. Wilkinson, S. G. Roberts, Ductile–brittle transition of polycrystalline iron and iron–chromium alloys. *J. Nucl. Mater.* **378**, 305–311 (2008).
16. E. Tarleton, S. G. Roberts, Dislocation dynamic modelling of the brittle–ductile transition in tungsten. *Philos. Mag.* **89**, 2759–2769 (2009).
17. V. Vitek, Core structure of screw dislocations in body-centred cubic metals: Relation to symmetry and interatomic bonding. *Philos. Mag.* **84**, 415–428 (2004).
18. B. Chen *et al*., Unusual activated processes controlling dislocation motion in body-centered-cubic high-entropy alloys. *Proc. Natl. Acad. Sci. U.S.A.* **117**, 16199–16206 (2020).
19. D. Caillard, On the stress discrepancy at low-temperatures in pure iron. *Acta Mater.* **62**, 267–275 (2014).
20. A. Seeger, Peierls barriers, kinks, and flow stress: Recent progress. *Z. Met.* **93**, 760–777 (2002).
21. L. Dezerald, L. Proville, L. Ventelon, F. Willaime, D. Rodney, First-principles prediction of kink-pair activation enthalpy on screw dislocations in bcc transition metals: V, Nb, Ta, Mo, W, and Fe. *Phys. Rev. B Condens. Matter Mater. Phys.* **91**, 094105 (2015).
22. P. Gumbsch, Brittle fracture and the brittle-to-ductile transition of tungsten. *J. Nucl. Mater.* **323**, 304–312 (2003).
23. A. Giannattasio, M. Tanaka, T. D. Joseph, S. G. Roberts, An empirical correlation between temperature and activation energy for brittle-to-ductile transitions in single-phase materials. *Phys. Scr.* **128**, 87–90 (2007).
24. Y. Li, X. B. Ren, J. Y. He, Z. L. Zhang, Constraint effect on the brittle-to-ductile transition of single-crystal iron induced by dislocation mobility. *Int. J. Mech. Sci.* **149**, 212–223 (2018).
25. C. St. John, The brittle-to-ductile transition in pre-cleaved silicon single crystals. *Philos. Mag.* **32**, 1193–1212 (1975).
26. D. Rupp, R. Mönig, P. Gruber, S. M. Weygand, Fracture toughness and microstructural characterization of polycrystalline rolled tungsten. *Int. J. Refract. Met. Hard Mater.* **28**, 669–673 (2010).
27. E. Bitzek, P. Gumbsch, Mechanisms of dislocation multiplication at crack tips. *Acta Mater.* **61**, 1394–1403 (2013).
28. C. Bonnekoh, A. Hoffmann, J. Reiser, The brittle-to-ductile transition in cold rolled tungsten: On the decrease of the brittle-to-ductile transition by 600 K to −65 °C. *Int. J. Refract. Met. Hard Mater.* **71**, 181–189 (2018).
29. C. Bonnekoh *et al*., The brittle-to-ductile transition in cold-rolled tungsten sheets: The rate-limiting mechanism of plasticity controlling the BDT in ultrafine-grained tungsten. *J. Mater. Sci.* **55**, 12314–12337 (2020).
30. L. Zhang, T. Ohmura, Plasticity initiation and evolution during nanoindentation of an iron-3% silicon crystal. *Phys. Rev. Lett.* **112**, 145504 (2014).
31. K. Durst, B. Backes, O. Franke, M. Göken, Indentation size effect in metallic materials: Modeling strength from pop-in to macroscopic hardness using geometrically necessary dislocations. *Acta Mater.* **54**, 2547–2555 (2006).
32. A. Gouldstone *et al*., Indentation across size scales and disciplines: Recent developments in experimentation and modeling. *Acta Mater.* **55**, 4015–4039 (2007).
33. W. C. Oliver, G. M. Pharr, An improved technique for determining hardness and elastic modulus using load and displacement sensing indentation experiments. *J. Mater. Res.* **7**, 1564–1583 (1992).
34. Y. F. Gu, H. Harada, Y. Ro, Chromium and chromium-based alloys: Problems and possibilities for high-temperature service. *JOM* **56**, 28–33 (2004).
35. W. H. Posil, W. C. Oliver, B. D. Fabes, The relationship between indentation and uniaxial creep in amorphous selenium. *J. Mater. Res.* **10**, 2024–2032 (1995).
36. B. N. Lucas, W. C. Oliver, Indentation power-law creep of high-purity indium. *Metall. Mater. Trans., A Phys. Metall. Mater. Sci.* **30**, 601–610 (1999).
37. W. W. Gerberich, S. K. Venkataraman, H. Huang, S. E. Harvey, D. L. Kohlstedt, The injection of plasticity by millinewton contacts. *Acta Metall. Mater.* **43**, 1569–1576 (1995).
38. A. S. Schneider *et al*., Correlation between critical temperature and strength of small-scale bcc pillars. *Phys. Rev. Lett.* **103**, 105501 (2009).
39. J. Li, K. J. Van Vliet, T. Zhu, S. Yip, S. Suresh, Atomistic mechanisms governing elastic limit and incipient plasticity in crystals. *Nature* **418**, 307–310 (2002).
40. J. Gagel, D. Weygand, P. Gumbsch, Formation of extended prismatic dislocation structures under indentation. *Acta Mater.* **111**, 399–406 (2016).
41. M. M. Chaudhri, "Dislocations and indentations" in *Dislocations in Solids*, F. R. N. Nabarro, J. P. Hirth, Eds. (Elsevier, 2004), vol. 12, pp. 447–550.
42. L. L. Li, I. J. Beyerlein, W. Z. Han, Interface-facilitated stable plasticity in ultra-fine layered FeAl/$FeAl_2$ micro-pillar at high temperature. *J. Mater. Sci. Technol.* **73**, 61–65 (2021).
43. D. Caillard, Geometry and kinetics of glide of screw dislocations in tungsten between 95K and 573K. *Acta Mater.* **161**, 21–34 (2018).